P2.1

THE EFFICACY OF SUBSIDENCE WARMING IN THE CORE OF NUMERICALLY SIMULATED TORNADO-LIKE VORTICES

Matthew R. Kumjian* and Brian H. Fiedler
School of Meteorology, University of Oklahoma, Norman, Oklahoma

1. INTRODUCTION

Lilly (1969) was the most notable advocate of subsidence warming in the core of tornadoes as an explanation for how tornadoes achieve such high wind speeds. Laboratory experiments (e.g., Church et al. 1979), numerical simulations (e.g. Walko 1988; Fiedler 1994), and observational studies (e.g., Wurman and Gill 2000) have shown that negative vertical velocities do occur in the cores of tornadoes; further, sometimes these downdrafts are quite vigorous. However, the central pressure deficit and maximum wind speed in observed and numerically simulated tornadoes frequently exceed the limits set by thermodynamic arguments. Simulations of axisymmetric vortices by Fiedler (1994, herein F94) show a core pressure deficit exceeding 30 times the CAPE-derived hydrostatic pressure drop, and an observational study by Samaras (2004) measured a 100-hPa pressure drop in the core of a violent F-4 tornado in South Dakota. Fiedler (1998, herein F98) and F94 have shown wind speeds up to five times the thermodynamic speed limit in simulated axisymmetric tornado-like vortices.

Despite numerous studies showing downdrafts in the cores of tornadoes, surprisingly few studies investigate the possible effects of subsidence warming on the maximum wind speeds and minimum central pressure. Walko (1988) and F94 looked into the plausibility of subsidence warming and agreed that most likely it occurs, yet these studies are inconclusive on the magnitude of the effect. In this simple project, the investigation of subsidence warming done in F94 will be revisited, but using a more natural configuration. A numerical model will be used to isolate the effects of subsidence warming and to conclusively quantify the significance of the warming on wind speeds and the vortex core pressure deficit in axisymmetric tornado-like vortices.

2. THE MODEL

As in Fiedler (1994), the numerical model utilized in this study is a primitive equation formulation of incompressible fluid motion within a cylindrical domain.

* *Corresponding author address*: Matthew R. Kumjian, National Weather Center, 120 David L. Boren Blvd., Room 5426, Norman, OK, 73072. Email: kumjian@ou.edu.

The cylindrical domain is expanded from F94, now with a rigid lid at $z = 2$ and a domain radius of $r = 4$. The entire domain rotates with angular velocity Ω. The dimensionless governing equations (in cylindrical coordinates):

$$\frac{\partial u}{\partial t} + u\frac{\partial u}{\partial r} + w\frac{\partial u}{\partial z} = \frac{v^2}{r} + 2\Omega v - \frac{\partial p}{\partial r} + \upsilon\left(\nabla^2 u - \frac{u}{r^2}\right) \quad (1)$$

$$\frac{\partial v}{\partial t} + u\frac{\partial v}{\partial r} + w\frac{\partial v}{\partial z} = -\frac{uv}{r} - 2\Omega u + \upsilon\left(\nabla^2 v - \frac{v}{r^2}\right) \quad (2)$$

$$\frac{\partial w}{\partial t} + u\frac{\partial w}{\partial r} + w\frac{\partial w}{\partial z} = -\frac{\partial p}{\partial z} + \alpha(t)b(r, z) + \beta s(r, z, t) + \upsilon\nabla^2 w \quad (3)$$

$$\frac{\partial ru}{\partial r} + \frac{\partial rw}{\partial z} = 0 \quad (4)$$

$$\frac{\partial s}{\partial t} + u\frac{\partial s}{\partial r} + w\frac{\partial s}{\partial z} = \upsilon\nabla^2 s \quad (5)$$

where *u, v,* and *w* represent the radial, tangential, and vertical components of the wind; 2Ω is the Coriolis parameter, υ is the dimensionless viscosity (and diffusivity), and *p* is the pressure divided by a constant density. F94 used a viscosity that increases with height. The present version uses a viscosity that is constant throughout the domain, which helps to alleviate numerical instabilities and the computational expense of increased resolution necessary for smaller viscosity values. Three values of υ are used: 0.0002, 0.0005, and 0.0010. The diffusion scheme, advection and derivative differencing are as in F94.

The velocity scale has been normalized using the thermodynamic speed limit and the length scale by the depth of the domain. Recall that the thermodynamic speed limit is the theoretical maximum vertical speed attained by a parcel in an environment with a fixed convective available potential energy (CAPE), obtained by integrating the approximated vertical equation of motion (i.e., only considering the buoyancy term):

$$w = \sqrt{2 \cdot CAPE} \quad (6)$$

A buoyant fluid is initially placed above z = 1, analogous to a stratosphere. In this model, the total buoyancy is

$$\alpha(t)b(r,z)+\beta s(r,z,t)\,, \tag{7}$$

while in F94 and F98 it is simply $b(r, z)$, where $b(r, z)$ is a buoyancy fixed in space, centered at z = 0.5. Here, the time-dependent factor $\alpha(t)$ multiplies $b(r, z)$, where $\alpha(t)$ ramps up from 0 at t = 0 to 1 at t = 20, thereafter remaining constant at 1. The fixed buoyancy $b(r, z)$ is given by

$$b(r,z) = 1.264\exp\left(-10r^2 - 20\left(z-0.5\right)^2\right) \tag{8}$$

such that integrating along the central axis results in the CAPE:

$$CAPE = \int_0^1 b(0,z) = 0.5 \tag{9}$$

As explained in F94 and F98, b is chosen such that (if acting alone) it could accelerate a parcel initially at rest at z = 0 to w = 1 at z = 1. Alternatively, b could support a hydrostatic pressure of p = -0.5 at z = 0. This would result in a maximum tangential wind speed v = 1 (the "thermodynamic speed limit") in cyclostrophic balance in an ideal potential vortex with a non-rotating core.

The additional buoyancy term new to this study is proportional to the scalar field $s(r, z, t)$, which is advected and diffused with the same diffusivity used for momentum. Below z = 1, s is initialized to be zero. Above z = 1, s is initialized as 1, except for a smooth transition zone centered on z = 1:

$$s(r,z,t=0) = \left[1+\exp\left((1-z)\kappa\right)\right]^{-1}, \tag{10}$$

where κ determines the sharpness of the transition zone. For all experiments in this study, κ = 30, which produces a moderate gradient of s in the transition zone.

The multiplicative factor β acting on s is essentially an inverse Froude number, or a measure of the buoyancy provided by s to the fixed buoyancy b, which drives the convection. The experiments done in this study vary β from 0 to 1, in increments of 0.2. For β = 0, the advective buoyancy s is analogous to a passive tracer. For β = 1, the "stratosphere" is quite warm. The total buoyancy field after the ramp up of α is shown in Figure 1.

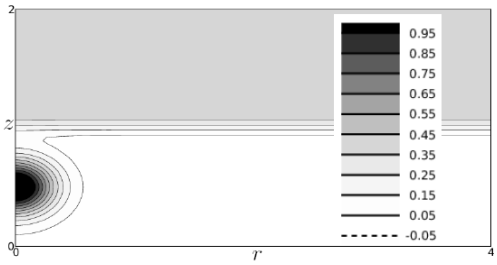

Fig. 1: Total buoyancy b(r, z) + βs(r, z, 0) with β = 0.4. The fixed buoyancy b(r, z) provides the elliptical contours centered on the axis at z = 0.5. The advective buoyancy s(r,z,0) is providing the upper layer of buoyancy. This is not the initial distribution of total buoyancy, but rather the total buoyancy that would be apparent after t = 20, once α = 1 and if s remains undisturbed (in reality s is disturbed by t = 20, so this is an idealized schematic of the two buoyancy sources in the model).

We can quantify the contribution of s to the hydrostatic pressure drop inside the vortex:

$$p_s = -\int_{z=0}^{z=2} \beta\, s(0,\,z,\,t)\,dz \;+\; 2\int_{r=0.5}^{r=1}\int_{z=0}^{z=2} \beta s(r,\,z,\,t)\,dz\,dr \tag{11}$$

This is the hydrostatic pressure drop supported by s on the central axis minus the hydrostatic pressure drop supported by s between r = 0.5 and r = 1. This pressure difference is what could augment the pressure gradient available for cyclostrophic balance.

In order to isolate the effects of subsidence warming from transient phenomena like suction vortices, the lower boundary is set to free-slip for all experiments. This prevents suction vortices and the vigorous vortex breakdown phenomena that commonly cause wind speeds to exceed 2, as in F94 and F98.

All experiments were run using a 91 x 91 stretched-grid domain except for those with the smallest value for viscosity; these were run on a 181 x 181 stretched-grid to alleviate instabilities. The grid points are stretched so that the highest resolution is at low-levels along the central axis (where the low-level wind speeds and pressure deficit of the tornado are of interest).

Table 1 below summarizes the parameters used for the 90 experiments. For each of the fifteen experiment numbers shown in the table, the inverse Froude number β is varied using the six values (0.0, 0.2, 0.4, 0.6, 0.8, 1.0).

Experiment Number	Viscosity (υ)	Coriolis (2Ω)
Exp1	0.0002	0.07
Exp2	0.0002	0.14
Exp3	0.0002	0.20
Exp4	0.0002	0.27
Exp5	0.0002	0.35
Exp6	0.0005	0.07
Exp7	0.0005	0.14
Exp8	0.0005	0.20
Exp9	0.0005	0.27
Exp10	0.0005	0.35
Exp11	0.0010	0.07
Exp12	0.0010	0.14
Exp13	0.0010	0.20
Exp14	0.0010	0.27
Exp15	0.0010	0.35

Table 1: Convention of Experiment numbers with indicated values of viscosity and ambient angular velocity. This convention is used for each value of β.

3. RESULTS

An example simulation is presented here with 2Ω = 0.2, υ = 0.0002, and β = 0.4. Figure 2 shows a time-series of the extrema of *v*, *p*, and p_s, and Figure 3 shows some fields midway through the simulation, at a time when subsidence warming in the core is providing 41% of the pressure drop at the surface.

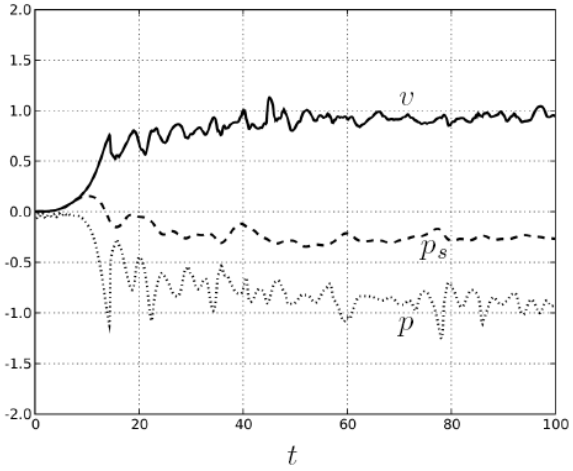

Fig. 2: Time history of the maximum in v and the minimum of p in the lower half of the domain. The contribution of s to the low pressure on the axis (p_s) can be thought of as a measure of subsidence warming.

The results of all ninety experiments are shown in Figure 4. Note that the averaging is over the window from 30 < *t* < 100. This is to filter out the instabilities associated with the initial spin-up of the vortex that occurs from 0 < *t* < 30. In other words, only the quasi-steady state fields are averaged.

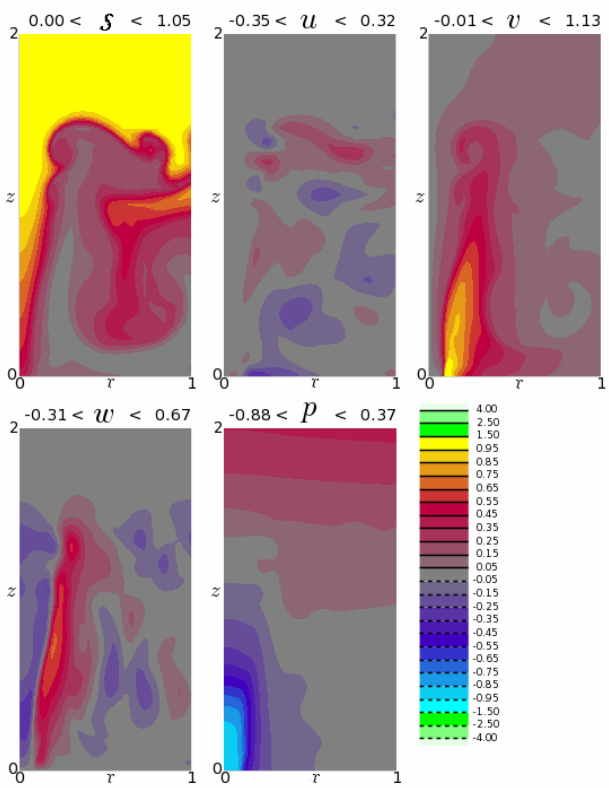

Fig. 3: Five panels showing the following variables at t = 45 in experiment when subsidence warming is contributing to about 41% of the pressure deficit, from left to right: the advective buoyancy s, radial velocity component u, tangential velocity component v, vertical velocity component w, and pressure perturbation p. At this time, the hydrostatic effect of βs is providing -0.35 of the -0.85 pressure difference at the surface between r = 0 and r = 1.

4. ANALYSIS AND DISCUSSION

Analyzing Figure 4, it is evident that the low viscosity experiments generally have significantly larger subsidence warming contributions to the core pressure deficit than the other experiments. The pattern becomes more pronounced with increasing *β*. It is possible that the increased viscosity causes increased "drag" that inhibits the vortex from ingesting as much of the highly-buoyant air. Quantitatively, the largest | p_s | ranges between about 0.35 and 0.41 for low viscosity experiments, 0.20 – 0.25 for medium viscosity, and 0.09 – 0.13 for the high viscosity experiments. The variations in Coriolis parameter provide a much smaller overall effect on the efficiency of subsidence warming.

The total pressure deficit does not appear to change significantly for *β* > 0. Taking the difference between the magnitude of the non-zero *β* pressure deficit and the control run *β* = 0 for each group of simulations,

$$\Delta \equiv \left|p(\beta > 0)\right| - \left|p(\beta = 0)\right| \qquad (12)$$

a statistical analysis can be performed. Using small-sample matched-pair confidence intervals at the 99% confidence level, a significant result would be a confidence interval that does not include zero. In other words, if the difference between pressure deficits with subsidence warming and the control runs is statistically insignificant, the confidence interval (which with 99% confidence contains the true difference Δ) will include zero. Table 2 below contains the results from the statistical analysis.

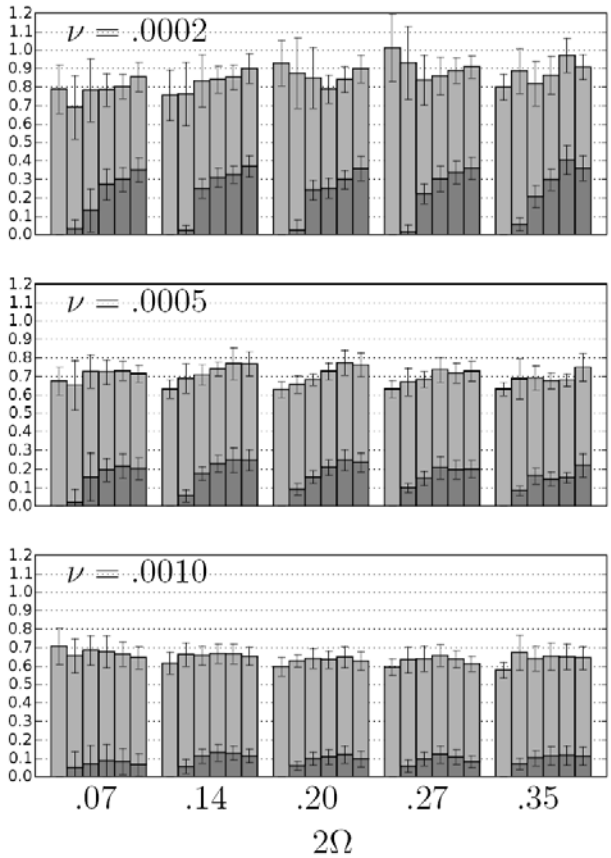

Fig. 4: Results from the ninety experiments: the gray bars are the average of the minimum of p for 30 < t < 100 from traces such as that shown in Fig. 2, plotted as the absolute value. The dark gray is the contribution of p_s. Error bars show the standard deviation over the model run. Each group of six experiments shows results for β equal to 0, 0.2, 0.4, 0.6, 0.8, and 1, from left to right. Experiments are separated by viscosity υ and Coriolis parameter 2Ω.

It is clear that using a 99% confidence interval, none of the samples show a statistically significant positive or negative difference. Next, the same statistical analysis is done for constant experiment number (from Table 1). The resulting 99% confidence intervals are shown in Table 3.

β	**99% Confidence Interval for Δ**
0.2	[-0.0337, 0.0582]
0.4	[-0.0319, 0.0728]
0.6	[-0.0314, 0.0934]
0.8	[-0.0151, 0.1115]
1	[-0.0037, 0.1109]

Table 2: 99% small-sample matched-pairs confidence intervals for constant β samples of the difference in magnitude of the pressure deficit between subsidence warming contributions and control run (no subsidence warming), defined as Δ.

Exp	**99% Confidence Interval for Δ**
1	[-0.1273, 0.1165]
2	[-0.0195, 0.1846]
3	[-0.1631, 0.0071]
4	[-0.2040, -0.0490]
5	[-0.0252, 0.2067]
6	[-0.0323, 0.1003]
7	[0.0314, 0.1772]
8	[-0.0120, 0.1967]
9	[0.0143, 0.1363]
10	[0.0040, 0.1275]
11	[-0.0742, -0.0084]
12	[0.0332, 0.0598]
13	[0.0210, 0.0582]
14	[0.0097, 0.0749]
15	[0.0485, 0.0996]

Table 3: As in Table 2, except for constant experiment number.

This time, several experiments (7, 9, 10, 12 – 15) show a statistically significant non-zero difference in magnitude of the pressure deficit between the $\beta > 0$ cases and the control run. To quantify how significant subsidence the contribution could be, consider Experiment 7. Assuming the most optimal conditions for subsidence warming, we will take the upper bound of the confidence interval to represent the maximum possible Δ, which is 0.1772. This corresponds to approximately a 71% increase in the magnitude of the core pressure deficit compared to the CAPE-derived hydrostatic pressure drop. However, since the pressure deficit in the core of the control simulation for Exp7 already exceeds the CAPE-derived hydrostatic pressure drop (see Fig. 4), the resulting contribution from subsidence warming corresponds to only a 28.1% decrease in the core pressure, slightly lower than estimates given by F94 and Walko (1988).

5. CONCLUSIONS

It is clear from this study and its predecessors (Walko 1988; F94) that subsidence warming does have a small effect on the pressure deficit in the core of a numerically-simulated tornado-like vortex. Under the most optimal conditions (which are unlikely to be satisfied in the real atmosphere), the magnitude of the pressure deficit increases by only about 30%. Because of the pressure deficit dependence on viscosity seen in these experiments, it is possible that lower viscosity experiments may show a greater effect; because the actual atmospheric viscosity is several orders of magnitude lower than the viscosity used in this study, it is possible that a larger subsidence warming-induced pressure deficit could occur in nature. However, it is unlikely that the effect would be significantly larger in nature, as the pressure deficits and maximum wind speeds in these simulations (and those of F94, F98) are comparable to those attained in real tornadoes.

Subsidence warming by itself does not have a significant impact on increasing the maximum wind speeds in tornado-like vortices. In fact, some of the wind speeds actually *decreased* as β was increased (not shown). Thus, subsidence warming as the explanation for the wind speeds in tornadoes exceeding the thermodynamic speed limit is not valid. In agreement with previous studies, we have found that subsidence warming in the core of the vortex appears to play an insignificant role in the evolution of tornado-like vortices, unlike in hurricanes. Instead, the explanation presented in Fiedler and Rotunno (1986) offers a purely dynamical explanation for the origin of supercritical wind speeds in tornadoes.

6. REFERENCES

Church, C.R., J.T. Snow, G.L. Baker, and E.M. Agee, 1979: Characteristics of tornado-like vortices as a function of swirl ratio: a laboratory investigation. *J. Atmos. Sci.*, **36**, 1755-1776.

Fiedler, B.H., 1994: The thermodynamic speed limit and its violation in axisymmetric numerical simulations of tornado-like vortices. *Atmosphere-Ocean*, **32,** 335-359**.**

———, 1998: Wind-speed limits in numerically simulated tornadoes with suction vortices. *Quart. J. Roy. Meteor. Soc.*, **124**, 2377-2392.

———, and R. Rotunno, 1986: A theory for the maximum windspeeds in tornado-like vortices. *J. Atmos. Sci.*, **33**, 2328-2340.

Lilly, D.K., 1969: Tornado dynamics. Technical Report NCAR Manuscript 69-117, National Center for Atmospheric Research.

Samaras, T.M., 2004: A historical perspective of in-situ observations within tornado cores. Preprints, *22nd Conf. on Severe Local Storms*, Hyannis, MA, Amer. Meteor. Soc., CD-ROM P11.4.

Walko, R.L., 1988: Plausibility of substantial dry adiabatic subsidence in a tornado core. *J. Atmos. Sci.*, **45**, 2251-2267.

Wurman, Joshua and S. Gill, 2000: Finescale radar observations of the Dimmitt, Texas (2 June 1995) tornado. *Mon. Wea. Rev.*, **128**, 2135-2164.